Aggregate WILEY

Au···I coinage bonds: Boosting photoluminescence efficiency and solid-state molecular motion

Xueqian Zhao[1,2] | Junyi Gong[3] | Zikang Li[1] | Herman H. Y. Sung[3] |
Ian D. Williams[3] | Jacky W. Y. Lam[3] | Zheng Zhao[4] | Ben Zhong Tang[3,4] |
Wai-Yeung Wong[1,2] | Linli Xu[1,2]

[1]Department of Applied Biology and Chemical Technology and Research Institute for Smart Energy, The Hong Kong Polytechnic University (PolyU), Hung Hom, Hong Kong, China

[2]PolyU Shenzhen Research Institute, Shenzhen, China

[3]Department of Chemistry, Hong Kong Branch of Chinese National Engineering Research Center for Tissue Restoration and Reconstruction, and Guangdong-Hong Kong-Macau Joint Laboratory of Optoelectronic and Magnetic Functional Materials, The Hong Kong University of Science and Technology, Kowloon, Hong Kong, China

[4]School of Science and Engineering, Shenzhen Institute of Aggregate Science and Technology, The Chinese University of Hong Kong, Shenzhen (CUHK-Shenzhen), Shenzhen, Guangdong, China

Correspondence
Wai-Yeung Wong and Linli Xu, Department of Applied Biology and Chemical Technology and Research Institute for Smart Energy, The Hong Kong Polytechnic University (PolyU), Hung Hom, Hong Kong, China.
Email: wai-yeung.wong@polyu.edu.hk and linli.xu@polyu.edu.hk

Abstract

Coinage bonds, a type of noncovalent interaction, occur between group 11 elements (Au, Ag, and Cu) with electron donor groups. Despite theoretical validation, empirical evidence remains limited. In this study, an aggregation-induced emission (AIE)-active Au(I) complex, **ITCPAu**, which exhibits Au···I coinage bonds, was revealed based on the single-crystal X-ray diffraction and theoretical calculations. Further examination of the luminescence properties of the **ITCPAu** revealed multiswitchable behavior, including mechanochromism and thermochromism. Nearly pure white-light emission was achieved with Commission Internationale de L'Eclairage (CIE) 1931 chromaticity coordinates of (0.30, 0.31) by grinding the green-emissive **ITCPAu** monomer crystals. Moreover, visualization and manipulation of solid-state molecular motion (SSMM) in the yellow-emissive **ITCPAu** dimer crystals, driven by the robust Au···I coinage bonds, were revealed through a combination of crystal engineering and luminescent properties. Furthermore, to support the robust Au···I coinage bonds, a versatile carrier for small solvent molecules in crystal lattices was developed for uptake and release. Our findings provide experimental and theoretical evidence for Au···I coinage bonds, highlighting their ability to boost photoluminescence quantum yield (PLQY) and trigger SSMM, emphasizing their potential in developing smart materials with stimuli-responsive properties.

KEYWORDS
Au···I coinage bond, solid-state molecular motion, stimuli-responsive material, white-light emission

1 | INTRODUCTION

Metallophilic interactions are prevalent in complexes and clusters of gold (Au), silver (Ag), and copper (Cu), and have long been a focus of research due to their significant effects on luminescence, alignment, and aggregation behavior in molecular and cluster studies.[1–7] In contrast, coinage interactions, also known as coinage bonds or regium bonds, are defined as the attractive forces between a coinage metal and an electron-rich unit and have only recently garnered much interest.[8] Despite sporadic reports[9–13] and theoretical predictions[14–16] of their existence, the understanding of coinage bonds remains limited, particularly regarding their effects on the relationship between structures and properties. Controlling the aggregation state of molecules and capturing the dynamics of molecular motion via coinage bonds would represent a major advance in this field.

Single-crystal X-ray diffraction (XRD) is a valuable tool for observing intercrystal transition patterns.[17–19] For example, Ito's group discovered a photo-induced single-crystal to single-crystal (SCSC) phase transition in Au(I) complexes, revealing the shortening of intermolecular aurophilic bonds.[20] However, detailed information about the molecular structure and packing of the amorphous phase cannot be obtained by XRD alone.[21] On the other hand, luminescence is a susceptible method that is not subject to external interference. Changes in luminescence color or intensity are strong indicators of changes in aggregation behavior in response to external stimuli triggered by various noncovalent interactions.[22,23] Aggregation-induced emission (AIE) has provided a general platform and research paradigm to study the influence of factors such as packing structure, admixture, intermolecular interactions, and aggregate morphology on the performance of macroscopic materials from the molecular to the aggregate level.[24–26] In a notable case, Tang and coworkers developed a pyrene-based molecule, (E)-2-[(pyren-1-ylimino)methyl]phenol (PIP), which displayed dim emission in the crystalline state but bright emission in the amorphous state due to strong $\pi\cdots\pi$ interactions in the crystalline state.[27] The reversible on/off emission could be finely tuned by scratching the crystalline film, allowing for the observation of fast and spontaneous solid-state molecular motion (SSMM) through changes in the fluorescence signals. These studies offer valuable tools and methods for examining the bonding in materials. They lay the groundwork for understanding how minor alterations in molecular structure and intermolecular interactions can result in significant changes in material properties, especially in luminescent materials.

In this study, we developed an AIE-active Au(I) complex, **ITCPAu**, which exhibited intermolecular Au⋯I coinage bonds that enhanced phosphorescent emissions and exhibited SSMM behavior. The remarkable luminescent property of **ITCPAu** in aggregate exhibited the green emission of the monomer and the yellow emission of the dimer. The stimuli-responsive behaviors of mechanochromism and thermochromism both in the **ITCPAu** monomer and dimer crystals were explored, nearly pure white-light emission through simple grinding of **ITCPAu** monomer was also achieved. The reversible photoluminescence (PL) quenching and recovery of the dimer crystals indicated their SSMM behavior. Furthermore, single-crystal XRD analysis revealed a significant Au⋯I distance of 3.457 Å within the **ITCPAu** dimer, and theoretical calculations corroborated the attractive nature of this noncovalent interaction. This work demonstrates that robust Au⋯I coinage bonds not only drive SSMM and boost photoluminescence efficiency but also enable the development of a versatile carrier within the crystal lattice for the uptake and release of small solvent molecules, providing a comprehensive understanding of Au⋯I noncovalent interactions.

2 | RESULTS AND DISCUSSION

2.1 | Synthesis and AIE properties of ITCPAu

We successfully synthesized the Au(I) complex **ITCPAu** with a high yield of 90% through the reaction of tris(4-chlorophenyl)phosphine Au(I) chloride with NaI at room temperature overnight.[28] The structure of **ITCPAu** is shown in Figure 1A, and the nuclear magnetic resonance (NMR) spectrum confirms its high purity (Figures S1–S3). The optical properties of **ITCPAu** in solution were initially characterized using ultraviolet–visible (UV–vis) absorption spectroscopy (Figure S4). The complex exhibited a distinct onset absorption at 275 nm. Further investigation into its AIE properties was conducted by examining its behavior in a dimethyl sulfoxide (DMSO)/water mixture with varying water fractions (f_w). As depicted in Figure 1B,C, the mixture exhibited negligible PL emission at low water fractions. However, when the water fraction reached 70%, the PL at 485 nm significantly intensified. This enhancement in PL is attributed to the aggregates of **ITCPAu**, as confirmed by dynamic light scattering (DLS) measurements shown in Figure 1D. Nanoparticles with a diameter of approximately 225 nm were observed in the DMSO/water mixtures with a water fraction of 70%. The restriction of intramolecular motion (RIM) mechanism is responsible for the AIE properties in the aggregate state.[29–32]

2.2 | Polymorph ITCPAu monomer and density functional theory results

Careful and slow crystallization from a dichloromethane/ethanol solution produced needle-like crystals with green PL under UV irradiation. The crystal structure of **ITCPAu** in the monomer phase was determined by the single-crystal XRD analysis (Figure 2A–C). The polymorph **ITCPAu** monomer exhibited a monoclinic space group $P21/n$, with a bond angle of 176.47° for the P–Au–I moiety, indicative of a near-linear configuration consistent with the geometry expected for an Au(I) complex.[33] The intermolecular CH⋯Cl hydrogen bond distances were measured at 2.892 Å and 2.765 Å, indicating weak hydrogen bonding interactions between neighboring molecules. In the **ITCPAu** monomer crystal, each molecule forms a zigzag structure, arranged in a head-to-tail pattern.[34] The large distance (7.51 Å) between the Au atoms of adjacent molecules indicates the absence of aurophilic interactions.[6] Density functional theory (DFT) calculations were performed based on the crystal structure of the **ITCPAu** monomer to analyze its electronic properties. As shown in Figure 2D, the highest occupied molecular orbitals (HOMOs; −5.93 eV) of the **ITCPAu** monomer are predominantly p orbitals localized on the I atom combined with d orbitals localized on the Au atom. The lowest unoccupied molecular orbitals (LUMOs; −1.83 eV) are $p*$ orbitals predominantly localized on the tris(4-chlorophenyl)phosphine ligand moiety. Thus, the lowest-energy absorption band observed in the stimulated UV–vis spectra (Figure S5) is attributed to the [1]LLCT and [1]MLCT transitions within the complex. The HOMO–LUMO energy gap computed for the **ITCPAu** monomer is 4.1 eV, which is in good agreement with the results from absorption spectroscopy (4.5 eV). Electrostatic potential (ESP) analysis was also performed on the **ITCPAu** monomer, as shown in Figure 2E. The isosurfaces of the ESP indicate the highly electron-rich nature of the I atom, revealing potential interaction sites with other electron-rich regions. The electron localized function (ELF) of the **ITCPAu** monomer was also
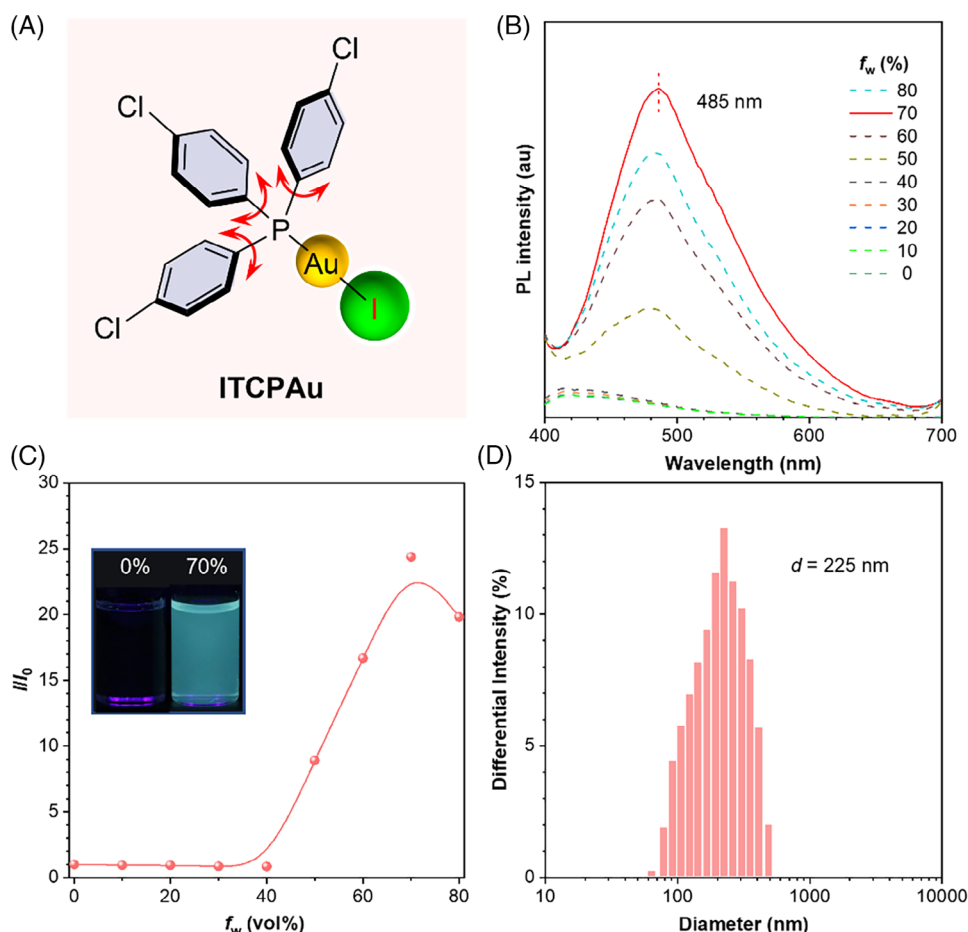
FIGURE 1 (A) Molecular structure of the iodo(tris(4-chlorophenyl)phosphine) Au(I) complex (**ITCPAu**). (B) Aggregation-induced emission (AIE) behavior of **ITCPAu** in a dimethyl sulfoxide (DMSO)/water mixture with varying water fractions (f_w). (C) Fluorescence intensity of **ITCPAu** at an emission wavelength of 485 nm as a function of f_w. The inset shows a comparative fluorescence photograph of **ITCPAu** in DMSO/water mixtures with 0% and 70% water fractions, illuminated by 365 nm ultraviolet (UV) light. (D) Dynamic light scattering (DLS) plot of **ITCPAu** particles in a DMSO/water mixture with a water fraction of 70%. PL, photoluminescence.

analyzed to identify regions of high electron localization, as depicted in Figure 2F. The bond orders for the Au–I and Au–P bonds are determined to be 1.0 and 0.7, respectively, suggesting a significant degree of electron localization at the I region.

2.3 | Au···I coinage bond and SSMM

Unlike the needle-like polymorph of the **ITCPAu** monomer, bulky crystals were obtained from a dichloromethane/methanol solvent mixture and were analyzed as the polymorph **ITCPAu** dimer by single-crystal XRD. The crystal belongs to the triclinic crystal system with the $P1$ space group. As shown in Figure 3A–C, the crystals exhibit a dimer stacking mode with two short Au···I distances of 3.457 Å. The intramolecular Au–I bond distances in the **ITCPAu** dimer (2.582 Å) are slightly longer than those found in the **ITCPAu** monomer (2.563 Å). The bond angle of the P–Au–I moiety (170.49°) indicates a greater distortion, suggesting a strong attraction between the Au and I atoms in the **ITCPAu** dimer. The presence of the Au···I coinage bond in the dimer was further evidenced by the yellow PL of the crystals, with an emission wavelength of 543 nm, as shown in Figure 3D. The absolute PL quantum yield (PLQY) reaches up to 70.5%, which is significantly higher than the

4.9% efficiency of the green-emissive **ITCPAu** monomer. The PL mechanochromism performance was investigated using fluorescence spectroscopy. The emission was gradually quenched upon grinding, with no shift in the emission peak. Powder XRD (PXRD) indicates that the destruction of the crystal structure is responsible for the yellow emission, as demonstrated in Figure 3E. Interestingly, the quenched fluorescence gradually recovers within hours, showing a certain degree of self-recovery capability. An increase in the ambient temperature to 70°C significantly accelerates the SSMM process, allowing recovery to the initial state within 100 s (Figure 3F). Additionally, the grinding and recovery cycle can be repeated multiple times, as depicted in Figure 3G.

2.4 | Multistimuli response and white-light emission

Upon grinding the **ITCPAu** monomer crystals, a noticeable PL mechanochromism was observed, as depicted in Figure 4A. The pristine **ITCPAu** crystal exhibits green luminescence with an emission peak at 504 nm. In contrast, the ground sample demonstrates white-light emission with two distinct peaks at 482 and 650 nm. The chromaticity coordinates for this white light are (0.30, 0.31) according to the Commission Internationale de L'Eclairage (CIE) 1931 color
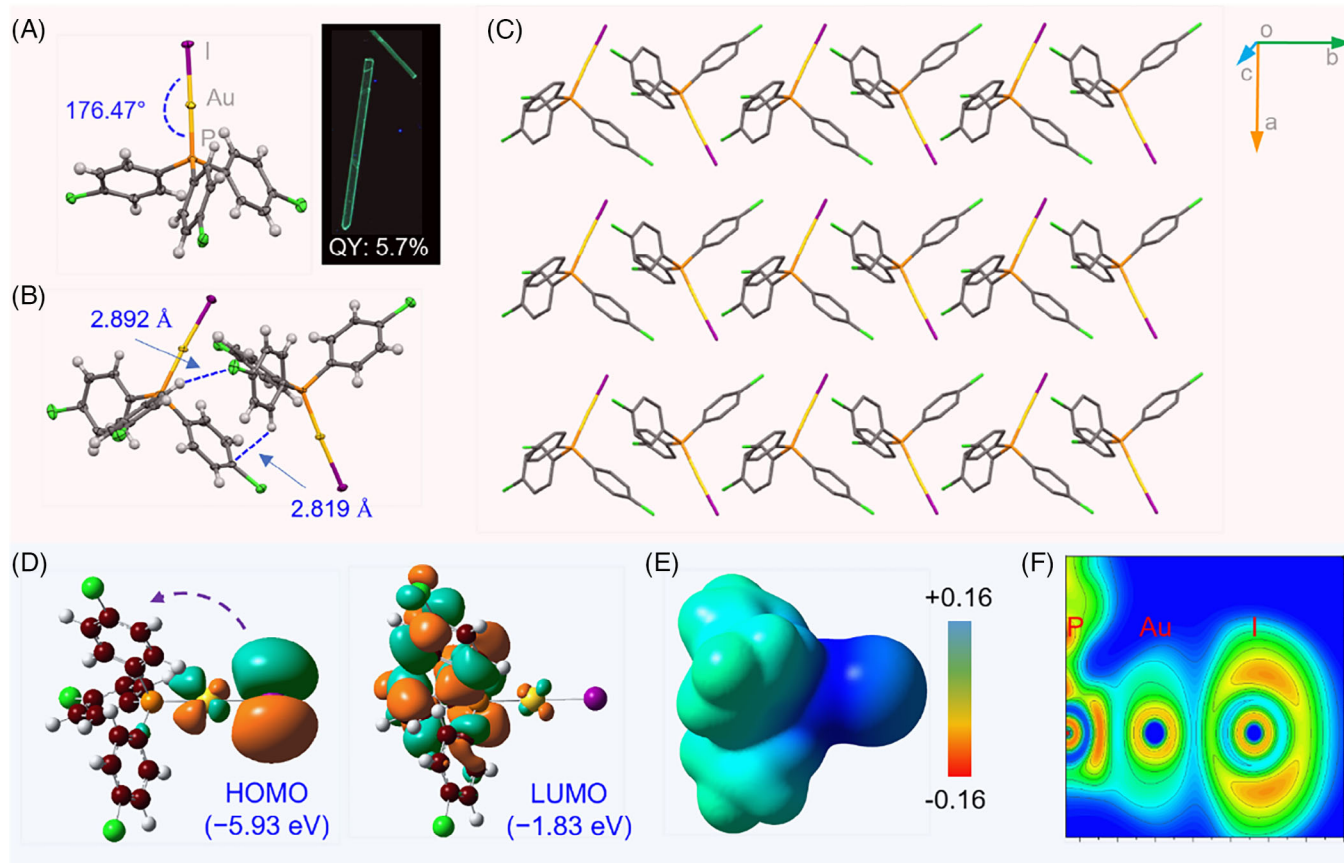
FIGURE 2 (**A**, **B**) Molecular structure and (**C**) molecular packing diagram of the **ITCPAu** monomer, shown with 50% probability ellipsoids. Hydrogen atoms are omitted for clarity. (**D**) Highest occupied molecular orbital (HOMO) and lowest unoccupied molecular orbital (LUMO) distribution, (**E**) electrostatic potential (ESP), and (**F**) electron localized function (ELF) of the **ITCPAu** monomer.
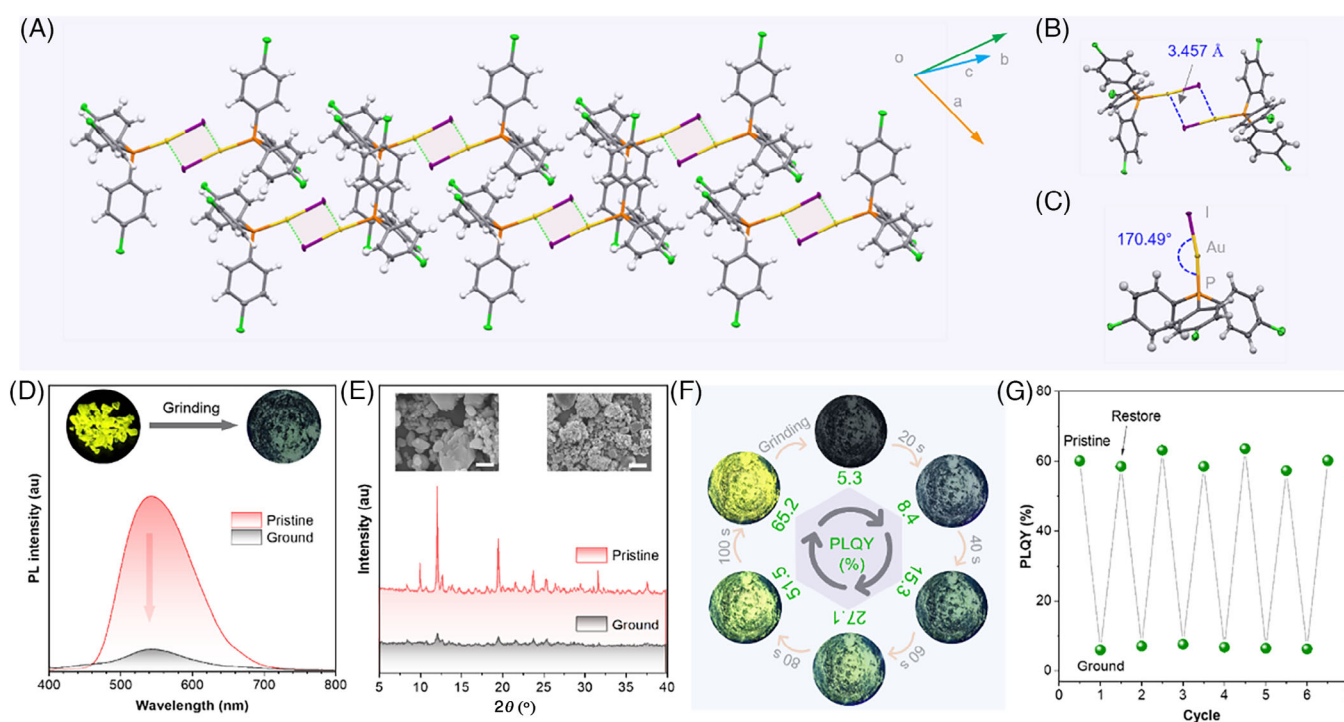

FIGURE 3 (**A–C**) Molecular packing and structure diagram of **ITCPAu** dimer, shown with 50% probability ellipsoids. (**D**) Photoluminescence (PL) spectra of the **ITCPAu** dimer in crystalline and ground states, along with an image of the solid sample of the **ITCPAu** dimer taken under ultraviolet (UV) irradiation before and after mechanical grinding. (**E**) Powder X-ray diffraction (PXRD) patterns of the **ITCPAu** dimer in crystalline and amorphous states, accompanied by corresponding scanning electron microscopy (SEM) images. (**F**) Fluorescence images of the ground **ITCPAu** dimer at different times at 70°C. (**G**) Recycling of emission intensities before and after grinding and heating. Excitation wavelength: 365 nm. PLQY, photoluminescence quantum yield.
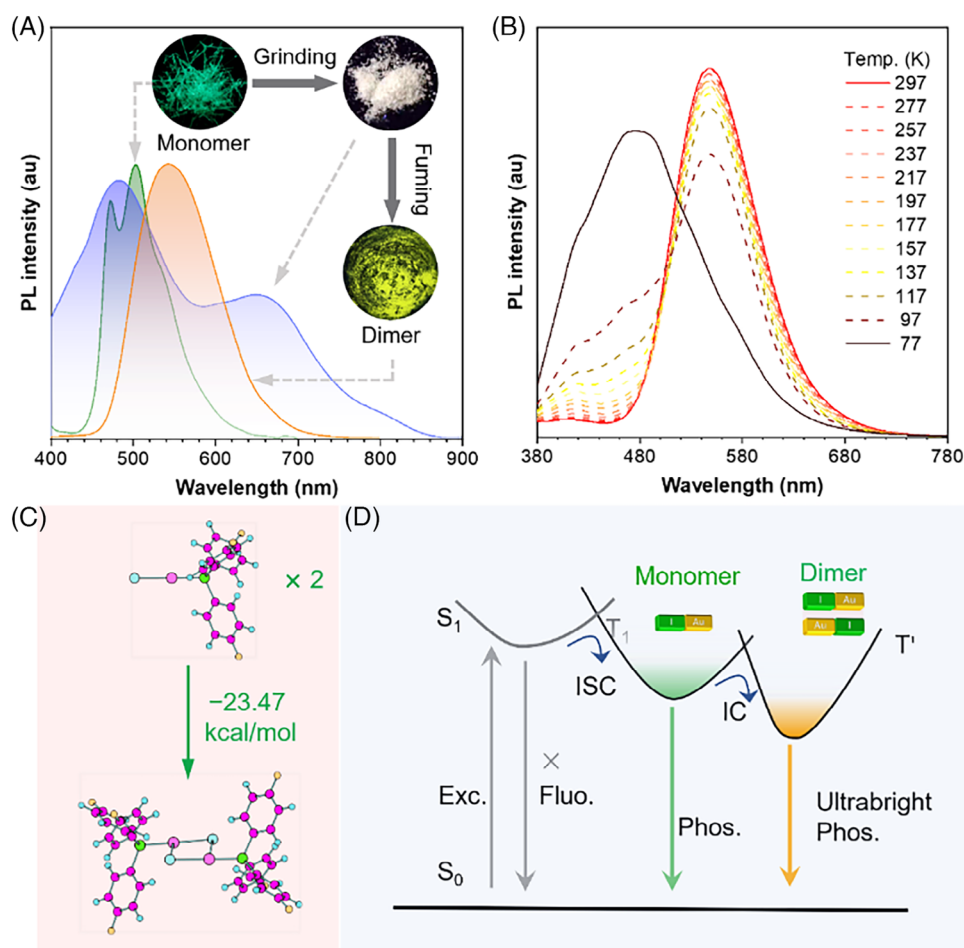
FIGURE 4 (A) Photoluminescence (PL) spectra of the **ITCPAu** monomer in crystalline, ground, and fumed states, along with images of the solid samples. (B) Variable-temperature emission spectra of the **ITCPAu** dimer in the range of 297–77 K. (C) Complexation energy of **ITCPAu**. (D) Schematic illustration of emission from the triplet state of the **ITCPAu** monomer and dimer. ISC, intersystem crossing; IC, internal conversion.

spaces.[35] The PXRD pattern of the pristine sample, shown in Figure S6, displays a well-ordered crystalline structure characterized by sharp peaks, indicative of the intactness of the monomer crystals. Conversely, the absence of these peaks in the PXRD pattern of the ground powders suggests a disruption of the original crystalline structure. The PL emission peak observed at 650 nm may be attributed to the formation of Au⋯Au interactions that could potentially occur during the grinding process, thus serving as the underlying cause for this observed spectral change.[36,37] Moreover, the ground white-light emissive samples did not revert to their initial state. After exposure to solvent vapor, they exhibited a significant yellow emission, suggesting the formation of the **ITCPAu** dimer species. Beyond the PL mechanochromic and solvatochromic properties of the **ITCPAu** monomer, the **ITCPAu** dimer also demonstrates a temperature-responsive PL emission (Figure 4B). Upon cooling, the yellow PL gradually diminishes, and by the time the temperature reaches 77 K, the yellow PL has entirely disappeared, replaced by green PL emission. This transition underscores the essential role of thermal activation in the emission of yellow PL, suggesting a temperature-induced change in the electronic states or molecular conformation that affects the PL emission properties.[38,39] To further verify the emission properties, we performed an analysis of the excitation spectra for the two luminescent crystal types, as shown in Figure S7. The excitation peak for the yellow emission was identified at 330 nm, whereas the green emission was excited

at 350 nm. This observation suggests that the yellow emission necessitates a higher energy input for excitation. We then measured the PL decay curves of the **ITCPAu** monomer and dimer crystals. Their lifetime profiles were similar, with their individual emissions evaluated to be on the microsecond scale. This indicates that both the green and yellow emissions can be ascribed to phosphorescence, as depicted in Figure S8. Notably, the lifetimes of the yellow emission peaks are about ten times shorter than those of the green emission peaks, with lifetimes of 3.7 ms for 472 nm and 0.36 ms for 543 nm, respectively. The lifetime of the ground-state **ITCPAu** dimer at 650 nm was also determined to be 18.3 ms, confirming its phosphorescent properties (Figure S9). The complexation energy of the present dimer is up to −23.47 kcal/mol according to the calculation results based on crystal structure, as shown in Figure 4C, indicative of a more robust dimer structure.[40] The **ITCPAu** monomer has a permanent dipole moment (PDM) of 7.8544 Debye, attributed to the strong electronegativity of the iodine atom. In contrast, the dimer's PDM is close to zero, indicating that the formation of the dimer is driven by dipole–dipole interactions. The greater polarizability of the dimer suggests that the intermolecular interactions within the dimer are stronger (Table S1). Here, we can see that the strong Au⋯I coinage interactions play a pivotal role in stabilizing the dimer and thus enhancing the yellow luminescence of the material, as demonstrated by the luminescence diagram in Figure 4D.
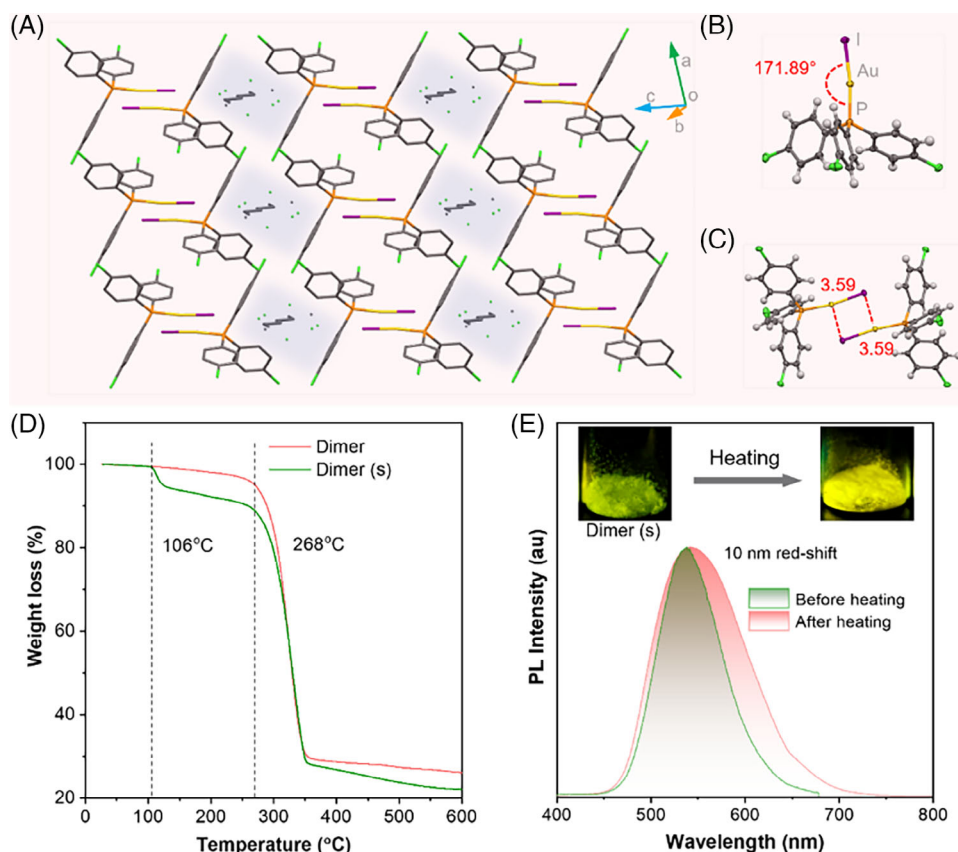
FIGURE 5 (**A**, **B**) Molecular structure and (**C**) molecular packing diagram of the **ITCPAu** dimer(s) with 50% probability ellipsoids. Hydrogen atoms were omitted for clarity. (**D**) Thermogravimetric (TG) curves of the **ITCPAu** dimer and dimer(s) at a heating rate of 10°C/min in a N_2 flow. (**E**) Photoluminescence (PL) spectra of the **ITCPAu** dimer(s) in pristine and heated states, and the corresponding images of the solid sample taken under ultraviolet (UV) irradiation.

2.5 | Small solvent molecule uptake and release

It should be noted that another yellow-emissive crystals exhibit one-dimensional (1D) pores, named as **ITCPAu** dimer(s), filled with a mixture of chloroform and *n*-hexane in a 1:2 volume ratio in Figure 5A. The crystal structure analysis elucidates the formation of these pores, providing insights into the unique architecture of the material. Figure 5B,C reveals the formation of the **ITCPAu** dimer with an Au⋯I distance of 3.59 Å. This confirms the hypothesis that Au⋯I coinage bonds serve as the primary force shaping the yellow-emissive crystalline phase. Thermogravimetric (TG) curves showed a rapid weight loss of about 5% at approximately 106°C–125°C for the dimer(s), signifying the release of the entrapped solvents (Figure 5D). This stability was maintained until the decomposition of the material beyond 268°C. This could also be monitored by fluorescence changes, as shown in Figure 5E. After heating, the PL spectrum became broader due to the increased flexibility of the **ITCPAu** dimer framework following the escape of solvent molecules. Based on these observations, we can conclude that the porous structure of the **ITCPAu** dimer(s) is not only realized but also capable of undergoing visual switching. The interplay between the Au⋯I coinage interactions and the induced yellow emission is directly responsible for the conformational changes observed in the material.

3 | CONCLUSION

In this work, we successfully synthesized an AIE-active Au(I) complex that exhibits multiple phosphorescent emissions and switchable behavior in various crystalline states. Specifically, the **ITCPAu** dimer crystal exhibits robust yellow emission at around 546 nm with a PLQY of 70.5%, while the monomer shows green emission at around 503 nm with a PLQY of 4.9%. By grinding the green-emissive **ITCPAu** crystals, we achieved nearly pure white-light emission with CIE coordinates of (0.30, 0.31). Disruption of the **ITCPAu** dimer crystals leads to fluorescence quenching, which is reversible within 100 s, as monitored by fluorescence variation, showcasing SSMM behavior. Analysis of the single-crystal structure revealed a significant Au⋯I distance of 3.457 Å in the **ITCPAu** dimer. Theoretical calculations supported the attractive nature of this noncovalent interaction, with a complexation energy of −23.47 kcal/mol, stronger than typical hydrogen bond. SSMM, as monitored by fluorescence verification, highlights the SSMM behavior driven by Au⋯I bonds. Additionally, the robust Au⋯I coinage bonds facilitate the development of a versatile carrier for small solvent molecules within the crystal lattice, enabling uptake and release. These findings provide a comprehensive understanding of Au⋯I noncovalent interactions and pave the way for further exploration and potential applications in materials science and photonics.

AUTHOR CONTRIBUTIONS

Xueqian Zhao performed all photophysical measurements, analyzed the data, synthesized the materials, and grew the crystals. Junyi Gong and Zikang Li performed the theoretical calculations. Herman H. Y. Sung and Ian D. Williams assisted in the analysis of the molecular crystal structure. Xueqian Zhao wrote the paper. Linli Xu and Wai-Yeung Wong contributed to the conceptualization and supervision. Jacky W. Y. Lam, Linli Xu, Wai-Yeung Wong, Zheng Zhao, and Ben Zhong Tang contributed to the review and editing. All authors discussed the results and commented on the manuscript.

ACKNOWLEDGMENTS

CONFLICT OF INTEREST STATEMENT

The authors declare no conflicts of interest.

PREPRINT STATEMENT

The research presented in this article was posted on a preprint server prior to publication in *Aggregate*. The corresponding preprint article can be found here: DOI: 10.26434/chemrxiv-2024-gql2x.

DATA AVAILABILITY STATEMENT

CCDC 2127920, 2127921, and 2127922 contain the supplementary crystallographic data for this paper. These data can be obtained free of charge via www.ccdc.cam.ac.uk/data_request/cif, or by emailing data_request@ccdc.cam.ac.uk, or by contacting The Cambridge Crystallographic Data Centre, 12 Union Road, Cambridge CB2 1EZ, UK; fax: +44 1223 336033. All data used to support the findings in the paper and Supporting Informations are available from the corresponding authors upon reasonable request. The Supporting Information is available at https://doi.org/10.1002/agt2.686.

ORCID

Junyi Gong https://orcid.org/0000-0001-7592-7132
Zheng Zhao https://orcid.org/0000-0002-5536-0439
Wai-Yeung Wong https://orcid.org/0000-0002-9949-7525
Linli Xu https://orcid.org/0000-0002-7032-9464

REFERENCES

1. K. He, Y. Jiang, T. Wang, Z. Liu, M. Wang, L. Pan, X. Chen, *Aggregate* **2022**, *3*, e57.
2. L. L. M. Zhang, W.-Y. Wong, *Aggregate* **2023**, *4*, e266.
3. Y. J. Wang, X. Y. Shi, P. Xing, S. Q. Zang, *JACS Au* **2023**, *3*, 565.
4. Q. Zheng, S. Borsley, G. S. Nichol, F. Duarte, S. L. Cockroft, *Angew. Chem. Int. Ed.* **2019**, *58*, 12617.
5. N. Goswami, Q. Yao, Z. Luo, J. Li, T. Chen, J. Xie, *J. Phys. Chem. Lett.* **2016**, *7*, 962.
6. H. Schmidbaur, A. Schier, *Chem. Soc. Rev.* **2012**, *41*, 370.
7. Z. Han, X. Zhao, P. Peng, S. Li, C. Zhang, M. Cao, K. Li, Z.-Y. Wang, S.-Q. Zang, *Nano Res.* **2020**, *13*, 3248.
8. K. T. Mahmudov, A. V. Gurbanov, V. A. Aliyeva, M. F. C. Guedes da Silva, G. Resnati, A. J. L. Pombeiro, *Coord. Chem. Rev.* **2022**, *464*, 214556.
9. M. K. Pandey, H. S. Kunchur, D. Mondal, L. Radhakrishna, B. S. Kote, M. S. Balakrishna, *Inorg. Chem.* **2020**, *59*, 3642.
10. M. L. N. Pina, A. Frontera, A. Bauza, *J. Phys. Chem. Lett.* **2020**, *11*, 8259.
11. H. Schmidbaur, *Angew. Chem. Int. Ed.* **2019**, *58*, 5806.
12. A. Daolio, A. Pizzi, G. Terraneo, M. Ursini, A. Frontera, G. Resnati, *Angew. Chem. Int. Ed.* **2021**, *60*, 14385.
13. A. S. Mikherdov, M. Jin, H. Ito, *Chem. Sci.* **2023**, *14*, 4485.
14. A. S. Novikov, *Inorg. Chim. Acta* **2018**, *471*, 126.
15. A. Avramopoulos, M. G. Papadopoulos, A. J. Sadlej, *Chem. Phys. Lett.* **2003**, *370*, 765.
16. J. Yan, Y. Zeng, L. Meng, X. Li, X. Zhang, *Phys. Chem. Chem. Phys.* **2023**, *25*, 29155.
17. S. Yang, P. A. Yin, L. Li, Q. Peng, X. Gu, G. Gao, J. You, B. Z. Tang, *Angew. Chem. Int. Ed.* **2020**, *59*, 10136.
18. M. Jin, T. Sumitani, H. Sato, T. Seki, H. Ito, *J. Am. Chem. Soc.* **2018**, *140*, 2875.
19. H. Ito, M. Muromoto, S. Kurenuma, S. Ishizaka, N. Kitamura, H. Sato, T. Seki, *Nat. Commun.* **2013**, *4*, 2009.
20. T. Seki, K. Sakurada, M. Muromoto, H. Ito, *Chem. Sci.* **2015**, *6*, 1491.
21. S. Liu, Y. Cheng, Y. Li, M. Chen, J. W. Y. Lam, B. Z. Tang, *ACS Nano* **2020**, *14*, 2090.
22. H. Wang, Q. Li, J. Zhang, H. Zhang, Y. Shu, Z. Zhao, W. Jiang, L. Du, D. L. Phillips, J. W. Y. Lam, H. H. Y. Sung, I. D. Williams, R. Lu, B. Z. Tang, *J. Am. Chem. Soc.* **2021**, *143*, 9468.
23. J. Zhang, B. He, W. Wu, P. Alam, H. Zhang, J. Gong, F. Song, Z. Wang, H. H. Y. Sung, I. D. Williams, Z. Wang, J. W. Y. Lam, B. Z. Tang, *J. Am. Chem. Soc.* **2020**, *142*, 14608.
24. Z. Zhao, H. Zhang, J. W. Y. Lam, B. Z. Tang, *Angew. Chem. Int. Ed.* **2020**, *59*, 9888.
25. Z. Zhao, C. Chen, W. Wu, F. Wang, L. Du, X. Zhang, Y. Xiong, X. He, Y. Cai, R. T. K. Kwok, J. W. Y. Lam, X. Gao, P. Sun, D. L. Phillips, D. Ding, B. Z. Tang, *Nat. Commun.* **2019**, *10*, 768.
26. H. Ou, S. Dai, R. Liu, D. Ding, *Sci. China Chem.* **2019**, *62*, 929.
27. P. Alam, N. L. C. Leung, Y. Cheng, H. Zhang, J. Liu, W. Wu, R. T. K. Kwok, J. W. Y. Lam, H. H. Y. Sung, I. D. Williams, B. Z. Tang, *Angew. Chem. Int. Ed.* **2019**, *58*, 4536.
28. E. R. T. Tiekink, J.-G. Kang, *Coord. Chem. Rev.* **2009**, *253*, 1627.
29. Y. Y. Liu, X. Zhang, K. Li, Q. C. Peng, Y. J. Qin, H. W. Hou, S. Q. Zang, B. Z. Tang, *Angew. Chem. Int. Ed.* **2021**, *60*, 22417.
30. M. M. Zhang, K. Li, S. Q. Zang, *Adv. Opt. Mater.* **2020**, *8*, 1902152.
31. J. Zhang, H. Zhang, J. W. Y. Lam, B. Z. Tang, *Chem. Res. Chin. Univ.* **2021**, *37*, 1.
32. Y. R. Hristova, B. Kemper, P. Besenius, *Tetrahedron* **2013**, *69*, 10525.
33. X. Y. Wang, J. Gong, H. Zou, S. H. Liu, J. Zhang, *Aggregate* **2023**, *4*, e252.
34. X. Zhao, J. Gong, P. Alam, C. Ma, Y. Wang, J. Guo, Z. Zeng, Z. He, H. H. Y. Sung, I. D. Williams, K. S. Wong, S. Chen, J. W. Y. Lam, Z. Zhao, B. Z. Tang, *CCS Chem.* **2022**, *4*, 1912.
35. J. Zhang, X. Zhao, H. Shen, J. W. Lam, H. Zhang, B. Z. Tang, *Adv. Photonics* **2022**, *4*, 014001.
36. T. Seki, N. Tokodai, S. Omagari, T. Nakanishi, Y. Hasegawa, T. Iwasa, T. Taketsugu, H. Ito, *J. Am. Chem. Soc.* **2017**, *139*, 6514.
37. X. Zhao, P. Alam, J. Zhang, S. Lin, Q. Peng, J. Zhang, G. Liang, S. Chen, J. Zhang, H. H. Sung, *CCS Chem.* **2022**, *4*, 2570.
38. N. Glebko, T. M. Dau, A. S. Melnikov, E. V. Grachova, I. V. Solovyev, A. Belyaev, A. J. Karttunen, I. O. Koshevoy, *Chem. Eur. J.* **2018**, *24*, 3021.
39. Z. Wu, Y. Du, J. Liu, Q. Yao, T. Chen, Y. Cao, H. Zhang, J. Xie, *Angew. Chem. Int. Ed.* **2019**, *58*, 8139.

40. A. Terron, J. Buils, T. J. Mooibroek, M. Barcelo-Oliver, A. Garcia-Raso, J. J. Fiol, A. Frontera, *Chem. Commun.* **2020**, *56*, 3524.

SUPPORTING INFORMATION

Additional supporting information can be found online in the Supporting Information section at the end of this article.